

# On the morse potential in liquid phase and at liquid-vapor interface

U.F. Galicia-Pimentel, D. Osorio-González, and J. López-Lemus<sup>a</sup>

*Facultad de Ciencias,  
Universidad Autónoma del Estado de México, Av. Instituto  
Literario 100, Toluca 50000, México,  
<sup>a</sup>e-mail: jllemus@uaemex.mx*

Recibido el 11 de mayo de 2006; aceptado el 27 de septiembre de 2006

Canonical Molecular Dynamics simulations have been performed to calculate thermodynamic properties in the liquid phase and at the liquid-vapor interface for fluids interacting by Morse potential. Transport properties such as self diffusion and shear viscosity have been calculated in one phase. Self diffusion shows an important dependence on particle number whereas shear viscosity does not show such dependence. At the liquid-vapor interface, properties such as orthobaric densities, vapor pressure, and surface tension were calculated. Equilibrium densities were compared with results obtained by NpT plus test particle method, and an excellent agreement was found. The surface tension and the vapor pressure are computed for the first time in this work. We also analyzed the cut-off distance dependence in both bulk and interfacial properties. No significant difference was found in the data obtained when two different cut-off distances were used,  $R_c = 2.5\sigma$  and  $R_c = 4.0\sigma$ . This is a consequence of the short-range nature of the potential.

*Keywords:* Surface tension; Morse potential; molecular dynamics.

Se realizaron simulaciones canónicas de Dinámica Molecular para obtener propiedades termodinámicas en la fase líquida y en la interfase líquido-vapor para fluidos que interactúan mediante el potencial de Morse. Se calcularon en una fase las propiedades de transporte tales como la autodifusión y la viscosidad de corte. La autodifusión muestra una dependencia en el número de partículas mientras que la viscosidad de corte no mostró tal comportamiento. Las propiedades que se calcularon en la interfase líquido-vapor fueron las densidades ortobaricas, la presión de vapor, y la tensión superficial. Las densidades de equilibrio fueron comparadas con aquellas densidades que se obtuvieron mediante la metodología NpT más partícula de prueba, y de esto se halló un acuerdo excelente. La tensión superficial y la presión de vapor se calculan aquí por primera vez. También hemos analizado la dependencia en el radio de corte por parte de las propiedades de bulto e interfaciales. Los datos obtenidos con dos distintos radios de corte,  $R_c = 2.5\sigma$  y  $R_c = 4.0\sigma$ , fueron comparados entre sí, y como resultado de ello, no hallamos diferencias significativas. Esto es una consecuencia de la naturaleza de corto alcance del potencial.

*Descriptores:* tensión superficial; potencial de Morse; dinámica molecular.

PACS: 31.15.Qg

## 1. Introduction

The Morse potential has been widely used for studying melting transition and laser ablation processes in computer simulation [1–3]. It has also exhibited advantages in the study of the fcc metals [4, 5]. Furthermore, there are several papers in the literature devoted to studying the structural properties of the Morse and Lennard-Jones (L-J) clusters, as well as the comparisons among them [3, 6–8]. In some cases, modifications on Morse function have been made [9–12] in order to improve the numerical results. Although traditionally the Morse potential has been employed to model covalent bonded diatomic molecules [13–15], it has also been used for estimating non-bonded interactions [16, 17]. This potential is qualitatively similar to that of L-J; however, they are quite different from a quantitative point of view. The L-J and Morse potentials can be compared in a direct manner by using a mathematical relationship that makes it possible to locate the minimum point of energy at the same position [18, 19]. In addition, it has been shown that it is possible to derive either one from the other [20].

It is important to analyze the liquid-vapor phase coexistence for simple or complex fluids, since it is closely related to real systems such as environmental processes or biological

systems, just to mention some examples. In the last decade, several studies on the liquid-vapor phase coexistence have been carried out by means of molecular simulation. In the case of the Morse potential, it is important to study its behavior in the bulk phase as well as in the liquid-vapor interface, because this would help us to have a broader view of the capabilities of this potential. Another important reason we are interested in the study of the liquid-vapor interface of the Morse potential is that in the near future, we would like to estimate interfacial properties of alkali metals using the Morse potential with a slight modification.

The Molecular Dynamics (MD) simulation technique is a successful tool for estimating thermodynamic properties in the bulk phase and at the liquid-vapor interface, mostly when the interface is physically present [21]. As is well known, an accurate calculation of the forces is fundamental obtaining reliable results of the properties mentioned above. In that sense, to clarify whether a large cut-off distance is necessary to calculate the full interaction for the Morse potential is one of the aims of this paper, which is relevant because it is difficult to include long-range corrections in transport properties during the simulations [22, 23]. Furthermore, the interfacial properties have shown an important dependence on the cut-off distance [24, 25]. Concerning the liquid-vapor properties, we

can see in the literature by using methods both with [24, 26] and without [27] interfaces, surface tension, vapor pressure, and coexisting densities in liquid-vapor interface have been estimated accurately, as is the case of the L-J potential [24]. For Morse fluids, the orthobaric densities have already been calculated in a previous work [19], but to our knowledge, data for vapor pressure and surface tension are not available for comparison. Besides, the dependence of the interfacial properties on the cut-off radius has not yet been analyzed.

In this work we calculate bulk liquid transport properties by MD simulations. We also perform interfacial simulations to estimate liquid-vapor properties for fluids interacting by Morse potential, the estimation of the surface tension being our main objective. The rest of the paper is organized as follows: in Sec. 2 we define the employed expression for the Morse potential, together with some relevant definitions. In Sec. 3 the simulation details are mentioned. The results are contained in Sec. 4. Finally, in Sec. 5 we include some concluding remarks.

## 2. Basic equations

To analyze the capabilities of Morse potential for calculating the interaction between two non-bonded particles, this potential is written in such a way that the minimum point of energy is in the same position as that of L-J potential [19, 20], which traditionally has been used to estimate the interactions of the Van der Waals type (see Fig. 1). The Morse potential is

$$\Phi = \epsilon \left[ 1 - \exp \left\{ \frac{-\ln(2)}{\sqrt[6]{2}-1} \left( \frac{r}{\sigma} - \sqrt[6]{2} \right) \right\} \right]^2 - \epsilon, \quad (1)$$

where the relationship  $r_e = 2^{1/6}\sigma$  has been used,  $\sigma$  being the effective diameter of particles and  $r_e$  the equilibrium pair

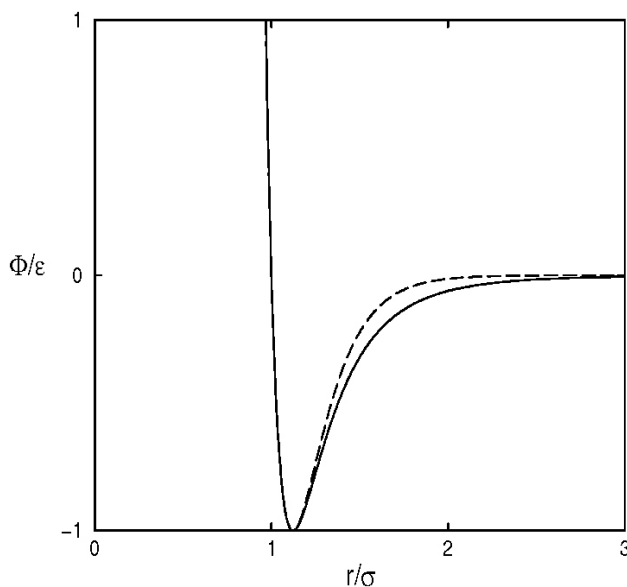


FIGURE 1. Comparison between L-J and Morse potentials. The continuous line corresponds to the former and the dotted lines represent the latter.

separation in the original expression. In Eq. (1),  $\epsilon$  is the depth of energy well and  $r$  is the distance between each pair of particles.

The Green-Kubo formulas have been used to calculate the transport properties in one phase [21]. The diffusion coefficient is written as

$$D = \frac{1}{3} \int_0^\infty \langle \mathbf{v}_i(0) \cdot \mathbf{v}_i(t) \rangle dt, \quad (2)$$

where  $\mathbf{v}_i$  is the velocity of particle  $i$ , and  $\langle \dots \rangle$  denotes the average ensemble. The expression for shear viscosity is

$$\eta = \left( \frac{V}{K_B T} \right) \int_0^\infty \langle P_{ij}(0) P_{ij}(t) \rangle dt, \quad (3)$$

where  $K_B$  is the Boltzmann's constant;  $V$  and  $T$  represent a given volume and temperature, respectively; and  $P_{ij}$  are the non-diagonal components of the pressure tensor. Indeed the components  $(\alpha\beta)$  of the pressure tensor are calculated by means of the virial expression

$$P_{\alpha\beta} V = \sum_{i=1}^N m_i \mathbf{v}_{i\alpha} \mathbf{v}_{i\beta} + \sum_{i=1}^{N-1} \sum_{j>i}^N (\mathbf{r}_{ij})_\alpha (\mathbf{f}_{ij})_\beta, \quad (4)$$

where  $m_i$  and  $\mathbf{r}_i$  are the mass and position of particle  $i$ , respectively. Hence  $\mathbf{r}_{ij} = \mathbf{r}_i - \mathbf{r}_j$ ,  $\mathbf{f}_{ij}$  is the force between two particles  $i$  and  $j$ .

The coexisting densities in the liquid-vapor equilibrium are calculated by fitting the density profiles  $\rho(z)$  to a hyperbolic tangent function

$$\rho(z) = \frac{1}{2}(\rho_L + \rho_V) - \frac{1}{2}(\rho_L - \rho_V) \tanh \left[ \frac{2(z-z_0)}{\delta} \right], \quad (5)$$

where  $\rho_L$  and  $\rho_V$  are the liquid and vapor densities, respectively. The thickness of the interface is  $\delta$ , and  $z_0$  is the Gibbs dividing surface. In addition, to estimate the critical temperature  $T_c$  and critical density  $\rho_c$ , we have used both the scaling law and the law of rectilinear diameters [28–30], in the same way as was done in Ref. 31. By using the equilibrium densities, the critical temperature is derived from the relation

$$\rho_L - \rho_V = A_1 \left( 1 - \frac{T}{T_c} \right)^\beta + A_2 \left( 1 - \frac{T}{T_c} \right)^{\beta+\Delta}, \quad (6)$$

where  $A_1$  and  $A_2$  are the correlation coefficients,  $\beta$  being the critical parameter with  $\beta = 0.325$  and  $\Delta = 0.5$ . Once the  $T_c$  is known, the critical density is estimated by using the law of rectilinear diameters,

$$\frac{1}{2}(\rho_L + \rho_V) = \rho_c + A_3 (T - T_c), \quad (7)$$

where  $A_3$  is an adjustable parameter.

To calculate the surface tension we used the mechanical definition

$$\gamma = \frac{L_z}{2} \left[ \langle P_{zz} \rangle - \frac{1}{2} \langle P_{xx} + P_{yy} \rangle \right], \quad (8)$$

where  $L_z$  is the side perpendicular to the interfacial area and  $P_{ii}$  are the diagonal components of the pressure tensor. Equation (8) has been divided by 2 because there are two interfacial areas.

### 3. Computational details

In all our simulations, the particles were placed in an fcc array. These were moved using the leap-frog algorithm implementing the periodic boundary conditions and minimum image convention in the three spatial directions [21]. In our simulations we employed two cut-off distances  $R_c = 2.5\sigma$  and  $R_c = 4.0\sigma$ . The temperature was maintained constant by normalizing the velocities at each step. The neighbor list was implemented in order to speed up the code.

In the liquid, phase the reduced hydrostatic pressure  $p^* = p\sigma^3/\epsilon$  and reduced potential energy  $U^* = U/N\epsilon$  were calculated for two different temperatures. We used  $N = 500$  particles changing the reduced density from  $\rho^* = \rho\sigma^3 = 0.1$  up to  $\rho^* = 0.9$ . The reduced temperatures were  $T^* = k_B T/\epsilon = 1.5$  and  $T^* = 2$ . In these simulations the time step employed was  $\Delta t = 0.005\sigma(m\epsilon)^{1/2}$ . By doing  $6 \times 10^4$  cycles, equilibrium was reached and performing  $3.4 \times 10^5$  cycles more, we calculated the averages of the pressure and energy. On the other hand, to calculate reduced self-diffusion  $D^* = D\sqrt{m}/\sigma$  and reduced shear viscosity  $\eta^* = \eta\sigma^2/\sqrt{m\epsilon}$  coefficients, a cubic cell was used with several particle numbers  $N = 256, 500, 864$  and  $2048$ . The reduced time step used was  $\Delta t^* = 0.0025$ . We used a reduced density of  $\rho^* = 0.81$  and a reduced temperature of  $T^* = 0.65$ , that corresponds to the liquid phase. The transport properties were estimated at the end of the simulations, storing the particle velocities and non-diagonal pressure tensor components every 10 time steps and every time step, respectively. In case of self diffusion, the number of particle velocities stored was  $N_{vel} = 256$  in all cases. In order to obtain the numerical values of transport coefficients, the time-dependent diffusion and time-dependent shear viscosity were evaluated at  $t^* = 1.5125$  and  $t^* = 1.5012$ , respectively. To reach equilibrium in the simulations, we performed  $5 \times 10^5$  integration steps, and to obtain averages, we carried out  $2 \times 10^6$  extra cycles.

Concerning the liquid-vapor interface, for the initial configuration a parallelepiped cell with a liquid slab surrounded by vacuum was considered. The side  $L_z^* = L_z/\sigma$  is perpendicular to the interface and it is larger than  $L_x^* = L_y^*$ . All the simulations were carried out using  $N = 1728$  particles. The adimensional time step was  $\Delta t^* = 0.005$ .  $5 \times 10^4$  cycles were performed to reach equilibrium, and  $1.45 \times 10^6$  cycles more were used to calculate the adimensional interfacial properties such as surface tension  $\gamma^*$ , vapor pressure  $P_V^*$ , liquid density  $\rho_L^*$  and vapor density  $\rho_V^*$ . It is important to clarify that in this work we are considering  $P_{ZZ}^* = P_V^*$ . In order to estimate the reduced surface tension confidently, we must pay attention to the oscillating behavior that shows this property when periodic boundary conditions and small

simulation boxes are employed. This oscillating behavior is exhibited for both polar and non-polar fluids when this property is calculated through the pressure tensor components. Indeed, dissipative particle dynamics simulations have also been performed to analyze the finite size effect on surface tension [33]. In case of polar fluids, this same procedure for estimating the surface tension could lead to unphysical results [32]. As was mentioned in Ref. 34, it is necessary to consider a large simulation box to avoid unreal results. Following these considerations, in this work we used a cell with  $L_x^* = 10 = L_y^*$ . Actually, for Morse potential, by using such system size, the oscillating behavior of this quantity vanishes.

### 4. Results

In this section we show the results obtained for Morse fluids by using molecular simulations. Figure 1 shows the comparison between L-J and Morse potentials; it is well-known that the range of the former is greater than that of the latter. By using Morse potential, (a) the pressure and (b) configurational energy in one phase were obtained; these results are contained in Fig. 2. Comparing the data obtained by using two different cut-off distances, we can observe that the largest difference on these properties is about 1.3% and it is located in pressure at a reduced density of 0.9 and a reduced temperature of 2.0.

Figure 3 shows (a) the reduced shear viscosity and (b) the reduced diffusion coefficient for several particle numbers by

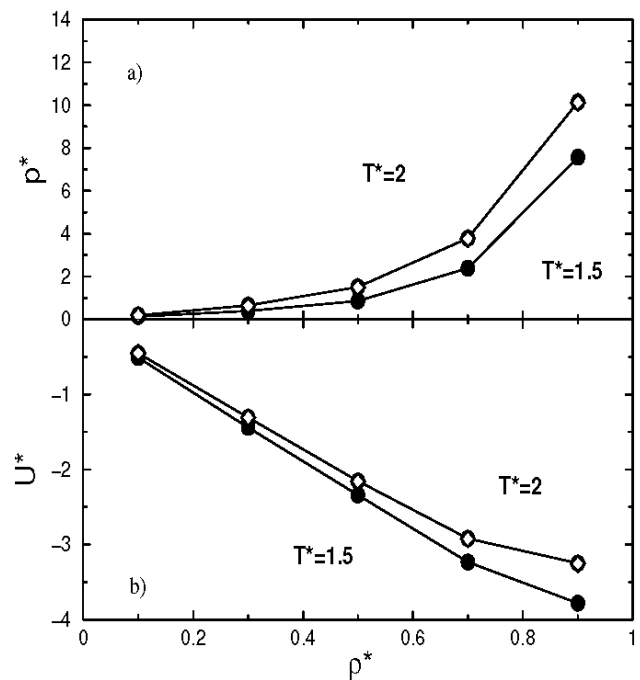


FIGURE 2. Reduced pressure (a) and reduced potential energy (b) are shown as a function of density. These results correspond to two different temperatures  $T^* = 1.5$  and  $T^* = 2$ . The filled circles and the open diamonds were obtained with  $R_c = 2.5\sigma$  and  $R_c = 4.0\sigma$ , respectively. The line was included just to guide the eye.

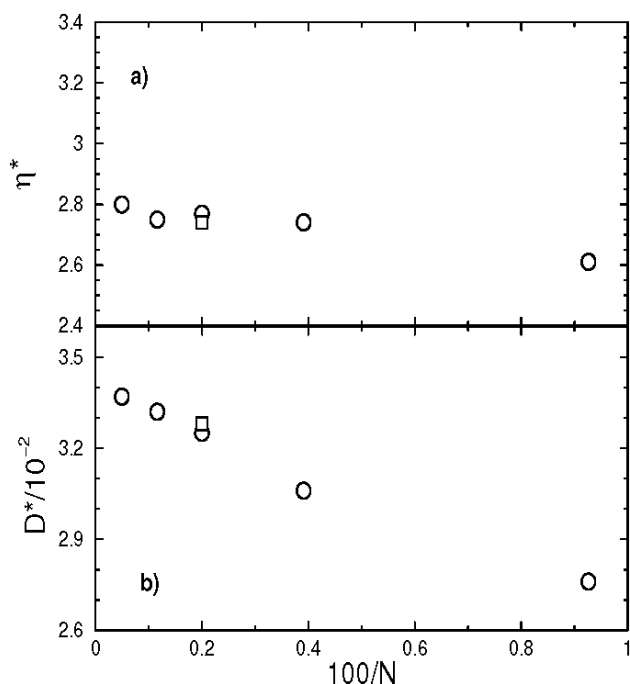


FIGURE 3. Reduced shear viscosity (a) and reduced self diffusion (b) plotted with particle numbers. The open circles and open squares correspond to results using  $R_c = 2.5\sigma$  and  $R_c = 4.0\sigma$ , respectively.

using two different cut-off distances. We notice that the self-diffusion depends on particle numbers while the shear viscosity does not show this same dependence, as in the case of the L-J fluid [24]. Added to this, these same transport properties do not show a clear dependence on cut-off distance. These data illustrate the short-range nature of Morse potential. Thus we can say that, by using a short cut-off distance, it is possible to calculate bulk properties accurately, and so it allows us to perform simulations with a small particle number for speeding up the process. For instance, the simulation performance by using  $R_c = 2.5\sigma$  is about 75% faster than that obtained with  $R_c = 4.0\sigma$ . When the transport properties were calculated by using two different cut-off distances, the resulting largest difference was about 1.4% and it corresponded to shear viscosity.

The results from this work for liquid-vapor interface are contained in Table I. Figure 4 shows the density profile  $\rho^*(Z/\sigma)$  as a function of the coordinate  $Z/\sigma$  which is normal to the interfacial area. These density profiles were calculated with  $R_c = 2.5\sigma$  and correspond to several reduced temperatures, 0.5, 0.6, 0.7 and 0.8 from top to bottom. The same kind of density profiles, not shown, are obtained for simulations by using  $R_c = 4.0\sigma$ . Figure 5 shows the equilibrium densities for Morse fluids. We compared our results with those obtained with NpT plus test particle method [19], and the agreement was excellent. In Fig. 5 are also plotted the data calculated by taking the arithmetic average  $(1/2)(\rho_V + \rho_L)$  of those densities obtained with  $R_c = 2.5$ . On the other hand, by means of the equilibrium densities obtained, the critical density and critical temperature were estimated in the same

TABLE I. Thermodynamic properties at liquid-vapor interface for Morse fluids. The particle number and the cut-off distance used were  $N = 1728$  and  $R_c = 2.5\sigma$ , respectively.

$T^*$	$\rho_V^*$	$\rho_L^*$	$P_V^*$	$\gamma^*$	$\delta/2\sigma$
0.45	0.0005	0.8770	0.00009	0.78 <sub>2</sub>	0.51
0.50	0.0009	0.8544	0.00040	0.68 <sub>2</sub>	0.64
0.55	0.0025	0.8296	0.00140	0.59 <sub>1</sub>	0.75
0.60	0.0056	0.8017	0.00350	0.49 <sub>1</sub>	0.84
0.65	0.0121	0.7712	0.00740	0.41 <sub>1</sub>	0.98
0.70	0.0200	0.7400	0.01230	0.32 <sub>1</sub>	1.14
0.75	0.0341	0.7042	0.02110	0.24 <sub>1</sub>	1.44
0.80	0.0525	0.6600	0.03290	0.16 <sub>2</sub>	1.68
0.85	0.0945	0.6063	0.04970	0.09 <sub>2</sub>	2.21
0.90	0.1503	0.5326	0.07210	0.03 <sub>2</sub>	4.15

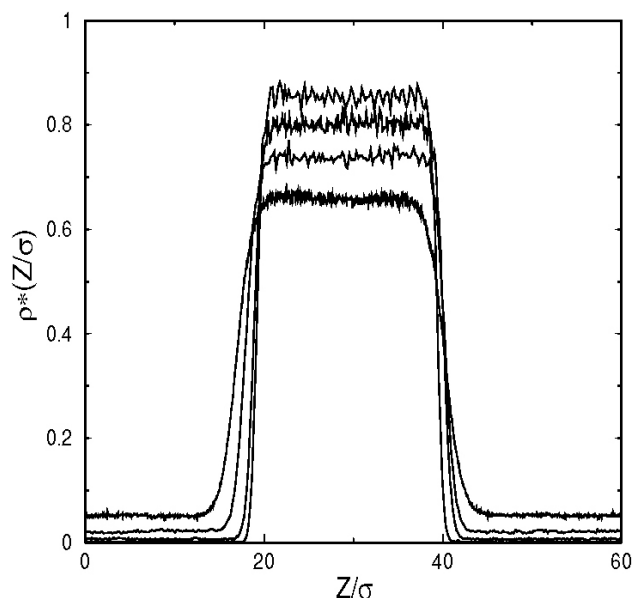


FIGURE 4. Reduced density profile for fluids interacting by Morse potential with  $R_c = 2.5\sigma$ .  $Z/\sigma$  is the reduced coordinate which is normal to the interfacial area. The reduced temperatures are 0.5, 0.6, 0.7 and 0.8 from top to bottom.

way as in Ref. 30. The obtained critical values for density and temperature were 0.334 and 0.931, respectively. These results were compared with those reported in Ref. 19, and the largest difference found was around 0.8% and it was located in density.

Figure 6 shows the logarithm of vapor pressure as a function of the inverse of the temperature. In Fig. 7, the surface tension is plotted as a function of temperature; this property behaves well when the density and temperature approach the critical point. In fact, the data obtained for both vapor pressure and surface tension are presented here for the first time. We want to emphasize that data for vapor pressure and surface tension were calculated by using two different cut-off radius, and as a result no significant difference was observed

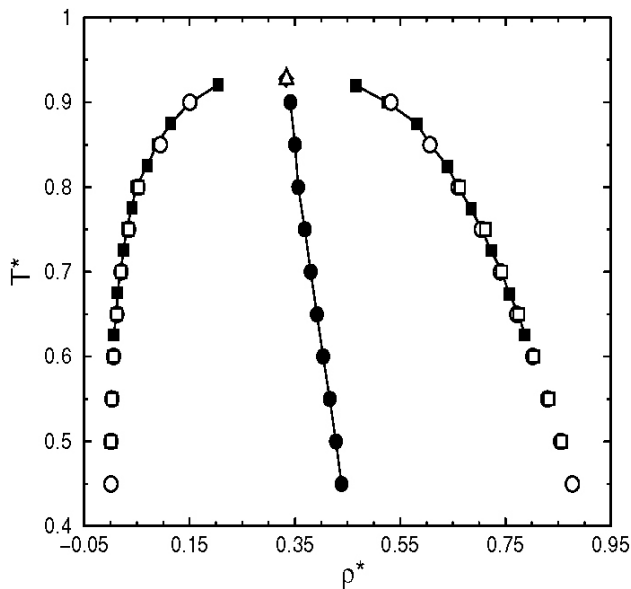


FIGURE 5. Reduced orthobaric densities against reduced temperature. The filled squares were taken from Ref. 19; they were estimated by using cut-off distances greater than  $4.0\sigma$ . The open circles and open squares are the results of this work using  $R_c = 2.5\sigma$  and  $R_c = 4.0\sigma$ , respectively. The filled circles correspond to the arithmetic average  $1/2(\rho_V + \rho_L)$  of those densities obtained by using  $R_c = 2.5\sigma$ . The open diamond corresponds to the result of the critical point taken from Ref. 19, and the open triangle was obtained from this work. The lines were included just to guide the eye.

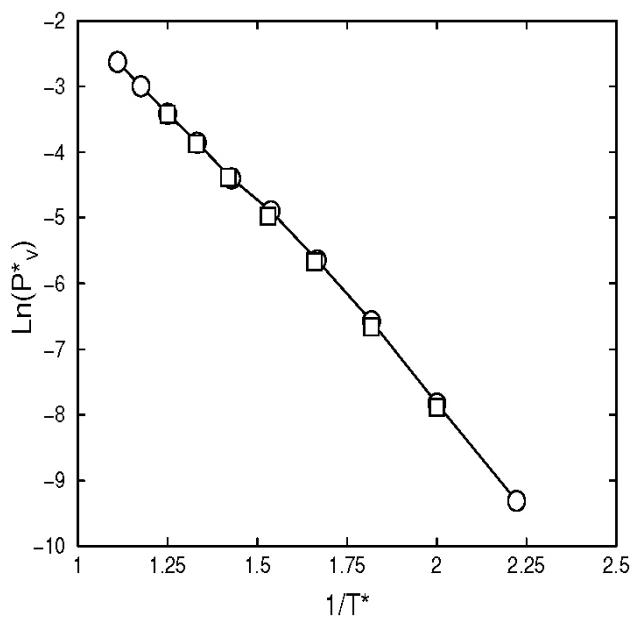


FIGURE 6. Logarithm of vapor pressure as a function of the inverse temperature. The symbols have the same meaning as in Fig. 5. The line was included just to guide the eye.

between them. This result was to be expected, since the Morse potential converges to zero at short distances. This kind of result is not observed with a L-J function because this potential converges to zero at greater distances; thus, in or-

der to take into account the full interaction, it is necessary to consider a large cut-off radius. In the same Fig. 7, there is a comparison between the surface tension obtained from Morse potential and that obtained from L-J potential. The difference is attributed to the long-range scope of the last potential.

As was pointed out by Gonzalez-Melchor *et al.* [35], an anisotropy is induced on pressure when the periodic boundary conditions are used employing a parallelepiped simulation box with considerably small interfacial area. As a direct consequence of this result, the surface tension shows an oscillating behavior for small system sizes, *i.e.*, when few particles are used. This same behavior can be observed in polar fluids as well [32]. In fact, for this kind of fluids the surface tension exhibits an anomalous behavior. This is a consequence of the estimation of this property through the pressure tensor by using small cross sectional areas. Hence, in order to obtain reliable results for surface tension here, we have considered that the interfacial area must be large enough [34]. Actually in Fig. 8 it the dependence of surface tension on interfacial area is shown. It is observed that with short boxes the oscillatory behavior is quite pronounced and, as soon as the simulation box is increased, this oscillation vanishes. This same behavior is exhibited by the  $L-J$  function as well [34]; when comparing the oscillatory behavior of the surface tension for both potentials, we can see that the oscillatory effect is greater for that potential with a greater range, as was mentioned in Ref. 35. Thus based on these results, we can stress that a cell with  $L_x^* = 10 = L_y^*$  is indeed large and appropriate. All our interfacial data were estimated by using two cut-off distances as well, and no important differences were found. This allows us to simulate interfacial properties such

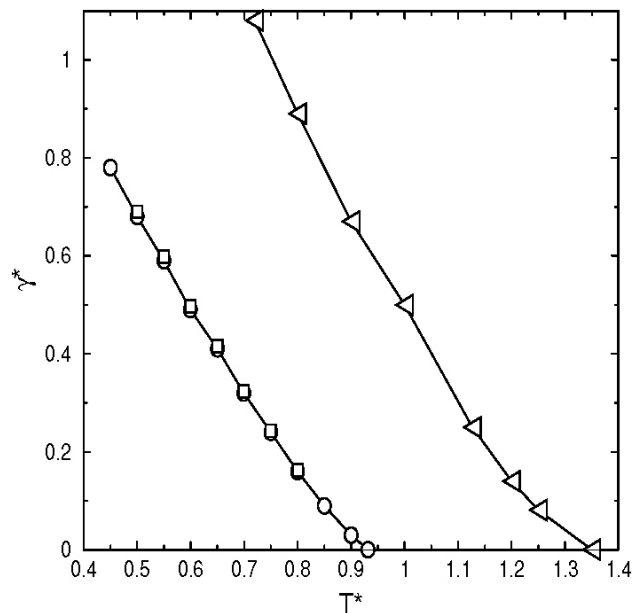


FIGURE 7. Reduced surface tension is plotted as a function of temperature. The left opened triangles were taken from Ref. 24 and were obtained using the full L-J potential. The other symbols have the same meaning as in Fig. 5. The line was included just to guide the eye.

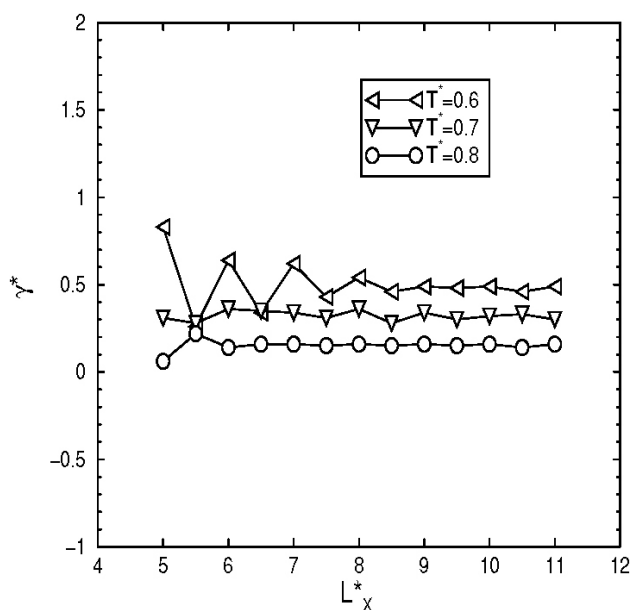


FIGURE 8. U.F. Galicia-Pimentel *et al*, *Rev. Mex. Fís.* (2006).

as surface tension and equilibrium densities by using a short cut-off distance. As a matter of fact, the finite size effect on the liquid-vapor coexistence curve has already been analyzed for simple [35] and molecular fluids [36], where it was emphasized that it is not necessary to have a large number of molecules to obtain good results. This is convenient because it is possible to analyze Morse fluid mixtures accurately, investing only a short computation time.

## 5. Concluding remarks

By means of Molecular Dynamics we have calculated transport properties in one phase and thermodynamic properties at the liquid-vapor interface.

As an important result in one phase, the shear viscosity and the self-diffusion are shown. They were estimated for a density and a temperature that correspond to the liquid phase. Concerning these properties, it is important to emphasize that self-diffusion depends noticeably on the particle

number and the shear viscosity does not present this dependence. The transport properties were calculated by using two different cut-off distances; the obtained data were compared among them and no significant difference was found. About this point, we can mention that both the velocity and pressure correlations decrease rapidly due to the short-range nature of the Morse potential.

On the other hand, the coexisting densities obtained were compared with those reported in Ref. 19, and good agreement was found. In agreement with earlier results [19], we located the critical point at  $\rho_c^* = 0.334$  and  $T_c^* = 0.931$ . A set of points were obtained by finding the arithmetic average on equilibrium densities  $(1/2)(\rho_V + \rho_L)$ ; this same set shows a linear behavior towards a critical point. In regard to the vapor pressure and surface tension results, we mention that there are no previous data to compare them with. We stress that the surface tension and vapor pressure do not depend on cut-off distance for fluids interacting by Morse potential; this fact takes relevance since surface tension has frequently shown a direct dependence on cut-off distance for both polar and non-polar fluids. Comparing both potentials, the Morse function has a shorter range than that of the  $L - J$  function; this difference directly affects the location of critical point and also the dependence of surface tension on temperature. According to Fig. 7, the difference on the critical point between both potentials is around 30%.

Finally, in the near future, we shall estimate transport properties in the liquid phase and interfacial properties in the coexistence of liquid-vapor phases for alkali metals, modeling them as simple structureless fluids, by modifying the Morse potential involving an extra adjustable parameter.

## Acknowledgments

The authors acknowledge CONACyT-México for partial support Grand P/49607. JLL wishes to thank UAEM-México Grands 2152/2005 and 2263/2006, for partial support. JLL would also like to thank Jorge Orozco-Velazco for his useful comments.

1. Y. Zhou, M. Karplus, K.D. Ball, and R.S. Berry, *J. Chem. Phys.* **116** (2002) 2323. And references therein.
2. X. Xu, C. Cheng, and I.H. Chowdhury, *J. Heat Transfer* **126** 727.
3. I. Last, Y. Levy, and J. Jortner, *PNAS* **99** (2002) 9107
4. L.A. Girifalco and V.G. Weizer, *Phys. Rev.* **114** (1959) 687.
5. S.J. Chen and H.L. Huang, *Chinese J. Phys.* **19** (1981) 106.
6. J.P.K. Doye and D.J. Wales, *Science* **271** (1996) 484.
7. J.P.K. Doye, R.H. Leary, M. Locatelli, and F. Schoen, *J. Comput.* **16** (2004) 371.
8. A. Tekin and M. Yurtsever, *Turk J. Chem.* **26** (2002) 627.
9. C.I. Chou, C.L. Ho, B. Hu, and H. Lee, *Phys. Rev. B* **57** (1998) 2747.
10. A. Strachan, T. Cagin, and W.A. Goddard III, *Phys. Rev. B* **60** (1999) 15084.
11. T.C. Lim, *Acta Chim. Slov.* **52** (2005) 149.
12. A. Del Sol Mesa C. Quesne and Y.F. Smirnov, *J. Phys. A* **31** (1998) 321.
13. P.M. Morse and E.C.G. Stueckelberg, *Phys. Rev.* **33** (1929) 932.
14. A.S. Leal, C. Gouvea dos Santos, C.M. Quintella, and H.H.R. Schor, *J. Braz. Chem. Soc.* **10** (1999) 359.

15. V. Constantoudis and C.A. Nicolaides, *J. Chem. Phys.* **122** (2005) 084118.
16. A.I. Milchev and A.A. Milchev, *Europhysics Lett.* **56** (2001) 695.
17. D. Osorio-González, M. Mayorga, J. Orozco, and L. Romero-Salazar, *J. Chem. Phys.* **118** (2003) 6989.
18. P. Shah and C. Chakravarty, *J. Chem. Phys.* **116** (2002) 10825.
19. H. Okumura and F. Yonezawa, *J. Chem. Phys.* **113** (2000) 9162.
20. T.C. Lim, *Z. Naturforsch.* **58a** (2003) 615.
21. M.P. Allen and D.J. Tildesley, *Computer Simulation of Liquids*, (Clarendon Press, Oxford, 1987).
22. D.M. Heyes, *Mol. Phys.* **71** (1990) 781.
23. M. Schoen and C. Hoheisel, *Mol. Phys.* **56** (1985) 653.
24. J. López-Lemus and J. Alejandre, *Mol. Phys.* **100** (2002) 2983.
25. A. Trokhymchuk and J. Alejandre, *J. Chem. Phys.* **111** (1999) 8510.
26. J. Janeček, *J. Phys. Chem. B* **110** (2006) 6264.
27. A.Z. Panagiotopoulos, N. Quirke, M. Stapleton and D.J. Tildesley, *Mol. Phys.* **63** (1988) 527.
28. F. Wegner, *Phys. Rev. B* **5** (1972) 4529.
29. J.V. Sebgers and J.M. Levelt-Sengers, *Progress in Liquid Physics* (C.A. Croxton. Wiley, Chichester, 1978).
30. L.J. Van Poolen, C.D. Holcomb and V.G. Nielsen, *Fluid Phase Equilib.* **129** (1997) 105.
31. J.K. Singh, D.A. Kofke and J.R. Errington, *J. Chem. Phys.* **119** (2003) 3405.
32. M. González-Melchor, F. Bresme and J. Alejandre, *J. Chem. Phys.* **122** (2005) 104710.
33. M.E. Velázquez-Sánchez, A. Gama-Goicochea, M. González-Melchor, M. Neria and J. Alejandre, *J. Chem. Phys.* **124** (2006) 084104.
34. P. Orea, J. López-Lemus and J. Alejandre, *J. Chem. Phys.* **123** (2005) 114702.
35. M. González-Melchor, P. Orea, J. López-Lemus, F. Bresme and J. Alejandre, *J. Chem. Phys.* **122** (2005) 94503.
36. J. López-Lemus, M. Romero-Bastida, T.A. Darden, and J. Alejandre, *Mol. Phys.* **104** (2006) 2413.